Copyright WILEY-VCH Verlag GmbH & Co. KGaA, 69469 Weinheim, Germany, 2019.

ADVANCED MATERIALS

# Supporting Information

for *Adv. Mater.*, DOI: 10.1002/adma.201901729

# Energy-Tailorable Spin-Selective Multifunctional Metasurfaces with Full Fourier Components

*Wenwei Liu, Zhancheng Li, Zhi Li, Hua Cheng, Chengchun Tang, Junjie Li, Shuqi Chen,* and Jianguo Tian*

Copyright WILEY-VCH Verlag GmbH & Co. KGaA, 69469 Weinheim, Germany, 2019.

# Supporting Information

## Energy-Tailorable Spin-Selective Multifunctional Metasurfaces with Full Fourier Components

*Wenwei Liu, Zhancheng Li, Zhi Li, Hua Cheng, Chengchun Tang, Junjie Li, Shuqi Chen*, and Jianguo Tian*

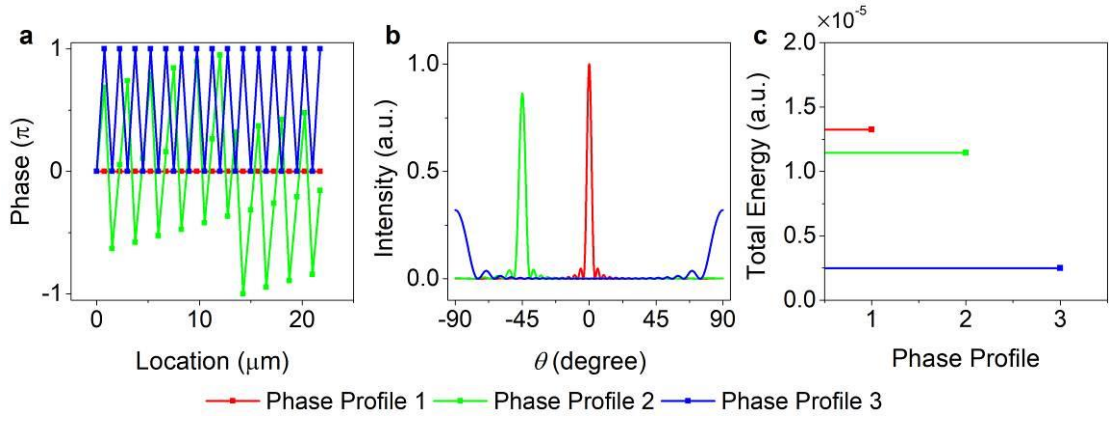


**Figure S1.** Calculated energy distributions for three phase profiles with unitary transmission in each unit cell. a) The three phase profiles are set as: $\phi_1 = 0$, $\phi_2 = k_x x$ with $k_x = k_0 \sin(45°)$, $\phi_3 = 0$ or $\pi$ for every other unit cell, respectively. b) The calculated intensity distribution[1] in angular space, where $\theta$ is calculated with $\arcsin(k_x/k_0)$ and $T^{MS}$ is set as 460 nm. c) Calculated total energy for the three phase profiles.

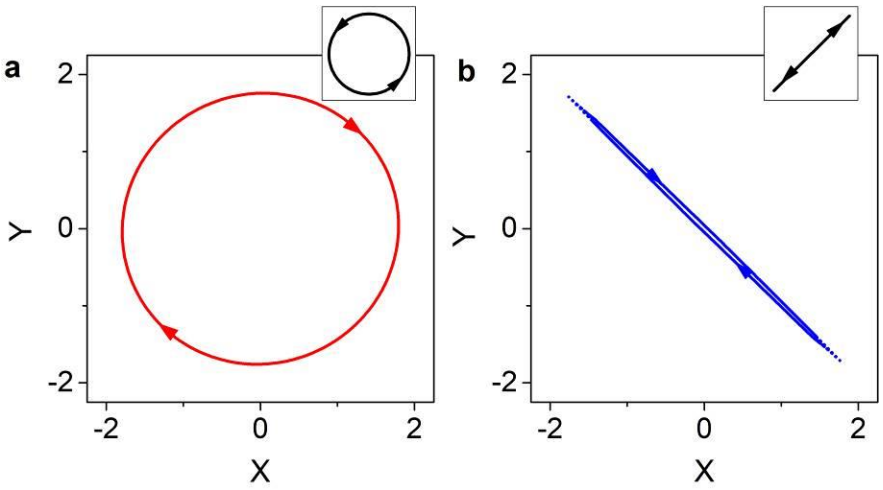


**Figure S2.** Simulated transmitted polarization states. a,b) The nanopillar with $a$ = 270 nm serving as a half-wave plate can convert the incident polarization to its orthogonal state with (a) LCP to RCP, (b) linear polarization to near-linear cross-polarization. The insets of (a) and (b) show the incident polarizations.

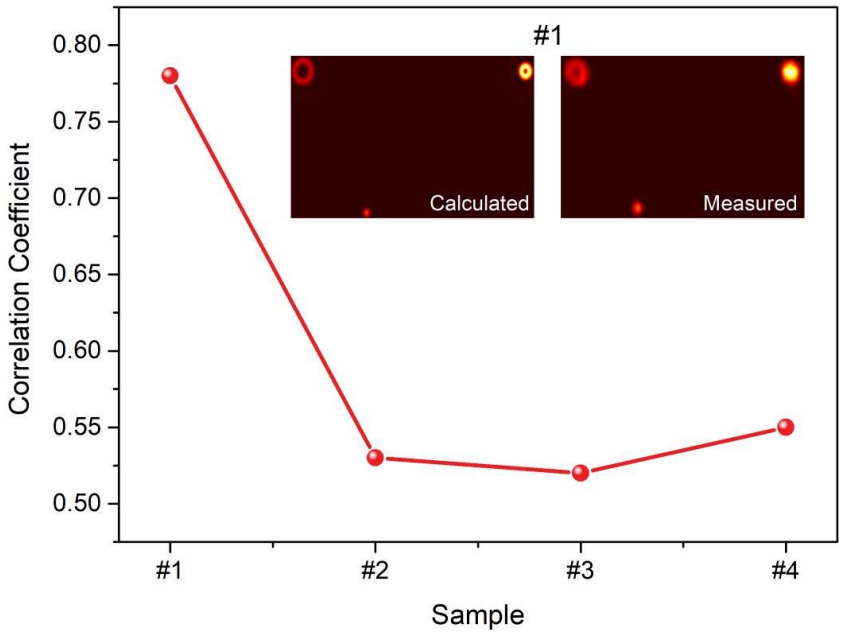


**Figure S3.** Calculated Pearson correlation coefficients between the theoretical and measured field distributions in *k*-space. Insets: theoretical $|E|^2$ and measured light distribution for Sample #1 after excluding the zero-order light.

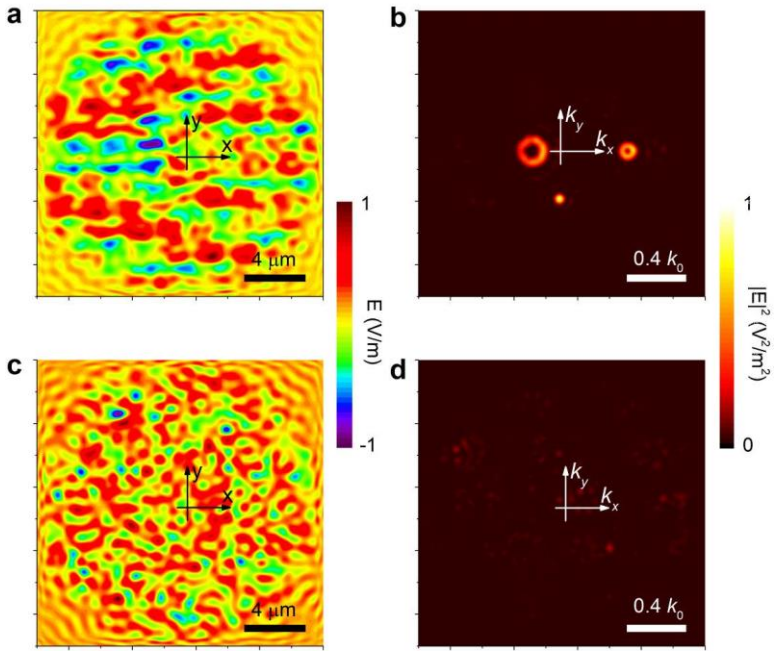


**Figure S4.** Simulated electric distributions in real space and *k*-space, where the radius of the metasurface is set as 16 μm. a) With LCP incidence, the simulated RCP field distribution at a cut plane with 5 μm from top of the nanopillars. b) Fast-Fourier transform (FFT) of the field distribution in (a) performed with MATLAB. c) With RCP incidence, the simulated LCP field distribution at a cut plane with 5 μm from top of the nanopillars. d) FFT of the field distribution in (c) performed with MATLAB.

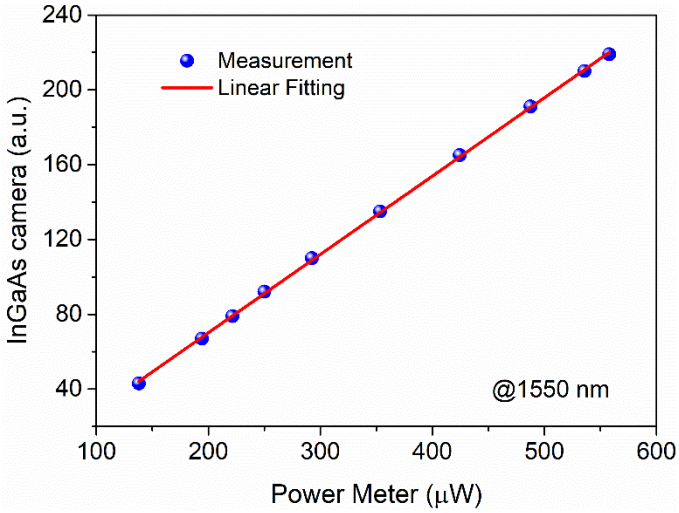


**Figure S5**. Comparison between the measured optical intensity with a power meter and with the InGaAs camera. The results show that the integrated intensity is linearly dependent on the actual light intensity, and the calculated R-Square parameter reaches

0.99977.

**S1. Function-related design**

The diffraction field distribution and total scattered energy of the metasurfaces are strongly related to the phase and strength of each unit cell. As shown in Figure S1, the highest energy corresponds to an identical phase distribution, while the energy of the diffraction field decreases for large phase gradients. This can be interpreted by summarizing two phase factor: $e^{i(\phi_i+kr_i)}+e^{i(\phi_i'+kr_i')}$, where $r_i$ and $r_i'$ is the locations of two neighboring unit cells. Defining phase gradient $\nabla\phi_i=\frac{\phi_i'-\phi_i}{r_i'-r_i}$ and position difference $\Delta=r_i'-r_i$, we obtain:

$$e^{i(\phi_i+kr_i)}+e^{i(\phi_i'+kr_i')}=e^{i(\phi_i+kr_i)}[1+e^{i(\nabla\phi_i+k)\Delta}], \quad (1)$$

which means an effective wave vector $k_i=\nabla\phi_i+k$ exists. This effective wave vector can be easily larger than $k_0$ for large phase gradient $\nabla\phi_i$, leading to evanescent waves that cannot propagate to far fields.

It is worth mentioning for hyperbolic media, this limitation can be relaxed since hyperbolic media can also manipulate large *k* components and evanescent waves.[2,3]

**S2. Pearson correlation coefficient of the measurements**

To evaluate the quality of the measured energy distribution, we calculated the Pearson correlation coefficients between the theoretical and measured light distributions (Figure S3). The Pearson correlation coefficient is defined as $corr(\mathbf{X},\mathbf{Y})=\frac{Cov(\mathbf{X},\mathbf{Y})}{\sqrt{Var(\mathbf{X})Var(\mathbf{Y})}}$, where **X**/**Y**, *Cov*(**X**,**Y**), *Var*(**X**) are an arbitrary numerical matrix, covariance of two matrices **X** and **Y**, variance of the matrix **X**, respectively. The Pearson correlation coefficient is a rigid parameter to characterize the linear similarity between two images. For sample #1, the Pearson correlation coefficient can reach a reasonable value of 0.78, considering the camera hardly recognizing the doughnut shape of the $F_2$ at the focal plane. The Pearson correlation

coefficients are also affected by the background noises in Figure 4g-j, which can be further improved by elaborate control of the fabrication conditions. During the calculation of Pearson correlation coefficient, we excluded the zero-order light in the measured intensity matrices, and the covariance analysis was performed to characterize the linear dependence between the theoretical and measured light distributions in *k*-space.

References

[1] W. Liu, Z. Li, H. Cheng, S. Chen, J. Tian, *Phys. Rev. Appl.* **2017**, *8*, 014012.

[2] P. Li, I. Dolado, F. J. Alfaro-Mozaz, F. Casanova, L. E. Hueso, S. Liu, J. H. Edgar, A. Y. Nikitin, S. Vélez, R. Hillenbrand, *Science* **2018**, *359***,** 892.

[3] I. Nefedov, A. Shalin, *Phys. Status. Solidi-R* **2017**, *11*, 1700219.